Enrichment of Chemical Element ^{7}Li in the Rotating Red Clump Star

Fang-Wen Wu(吴方文)[1], Han-Feng Song(宋汉峰)[1,2*], Qing-Li Li(李清莉)[1], Yun He(何云)[1], Xin-Yue Qu(曲新玥)[1], and Zhuo Han(韩卓)[1]

[1]*College of Physics, Guizhou University, Guiyang 550025, China*
[2]*Geneva Observatory, University of Geneva, CH-1290 Sauverny, Switzerland*

(Received 4 June 2024; accepted manuscript online 25 July 2024)

About 2 percent of red clump stars are found to be the lithium-rich and thus the surface lithium increases obviously in some red clump stars. The physical mechanism of the lithium enrichment in these stars has not yet been explained satisfactorily by the evolutionary models of single stars. The flash induced internal gravity wave mixing (i.e., IGW) could play a primary role in explaining the red clump star with lithium enrichment and it has a very significant impact on the internal structure and surface compositions of a star. Rotation can significantly increase the mixing efficiency of the internal gravity wave because the timescale for the enrichment event has been enlarged. Thermohaline mixing can explain the observed behavior of lithium on red giant stars that are more luminosity than the RGB bump. However, it has a very small effect on the diffusion of elements because its diffusion coefficient is much smaller than the one of IGW induced mixing after the core helium flash.

DOI: 10.1088/0256-307X/41/8/089701

Research on stellar nucleosynthesis and evolution is an important topic in stellar astrophysics.[1–3] Lithium is one of stable species which can be produced in a significant quantity during big bang nucleosynthesis.[4] When the local temperature in a star outweighs 2.5×10^6 K, ^{7}Li can be depleted by capturing the proton via the nuclear reaction ^{7}Li(p, ^{4}He)^{4}He. Therefore, lithium can only be retained inside the cool region of the star which is located at stellar outer envelope or the atmosphere. Generally, the interstellar medium has the initial lithium abundance of ($A_{\rm Li} = \log_{10}(N_{\rm Li}/N_{\rm H}) + 12 \sim 3.3\,{\rm dex}$). $N_{\rm X}$ refers to the number density of atoms of a species. However, a star with an initial lithium abundance in the interstellar medium has a surface value which is less than 1.5 dex after the first dredge-up in the red giant star branch.

Yan *et al.*[5] found that about 150 Li-rich giants with $A_{\rm Li} \geq 1.5\,{\rm dex}$ have been found in the past years and about 20 of them were found to be super Li-rich stars with $A_{\rm Li}$ higher than 3.3. However, over the following years, this number has dramatically increased due to spectroscopic surveys such as LAMOST and GALAH, encompassing over 10000 stars.[4,6] Recently, Martell *et al.*[6] have investigated the properties of 1262 red giant stars with high photospheric abundances of lithium observed by the GALAH and K2-HERMES surveys. They confirmed that Li-rich giants are rare, making up only 1.2 percent of giant star sample. They also found that red clump stars are 2.5 times as likely to be lithium-rich as RGB stars. Yan *et al.*[7] revealed that the majority of lithium-rich stars are confirmed to be red clump stars, whereas red giant stars are minor. Red clump stars have an enhancement in lithium that is a factor of about 40 above the value near the tip of the red giant branch. The most lithium-rich giant star has been shown to possess $A_{\rm Li} \geq 4.5\,{\rm dex}$.[5]

The physical mechanism of the enrichment of lithium-rich giants has not yet been explained satisfactorily by the evolutionary models of single stars. At present, three main scenarios have been proposed to explain these lithium-enriched giants. The first scenario is that the lithium can be obtained from a rocky planet or brown dwarf companion.[8,9] The second one is that lithium-rich matter has been accreted from a nova or an asymptotic giant branch companion star (Aguilera-Gòmez *et al.*[8]). The final scenario is that the lithium has been generated in the interior of the star and very rapidly transferred to the surface by the extra mixing mechanism.[5,10] The fresh lithium may be generated by the Cameron Fowler mechanism, in which lithium is produced following the nuclear reaction ^{3}He(α, γ)^{7}Be and then beryllium ^{7}Be is believed to be transferred from the hydrogen-burning shell to a cooler region where it may be changed into lithium by β-capture ^{7}Be(e^-, ν)^{7}Li. In this scenario, the actual physical mechanism that triggers the mixing plays an important role. Several extra mixing mechanisms have been proposed, including rotational induced mixing, the mixing induced by thermohaline mixing, and the mixing induced by the internal gravity waves.[11] The formation channels of lithium-rich red giants are not yet known.

In this Letter, we intend to explore how rotation, thermohaline mixing and internal gravity waves can change the surface chemical abundance of lithium-rich red giant stars. We aim to explore the following questions in the rotating star scenario: (1) How do initial rotational velocities have an impact on the formation of lithium-rich red clump stars? (2) How can the mixing effect of internal gravity waves explain the Li abundance distribution and evolution of red clump stars with low-mass progenitors?

The Initial Parameters and Model Descriptions. The

*Corresponding author. Email: hfsong@gzu.edu.cn
© 2024 Chinese Physical Society and IOP Publishing Ltd

model presented in this investigation has been calculated with the MESA code (release: version 10398, Bill *et al.*[12–15]). We use the Schwarzschild criterion to determine the boundaries of the convective region. Convection is modeled using the standard mixing length theory [Böhm-Vitense (1958);[16] Cox and Giuli (1968)[17]] prescription with a mixing length parameter of $\alpha_{\rm MLT} = 1.5$, following Pols *et al.*[3] The mixing length is $l_{\rm m} = \alpha_{\rm MLT} H_{\rm P}$, where $H_{\rm P}$ is the pressure scale height at the outer boundary of the core. We consider convective core-overshooting adopting an overshooting parameter of 0.25 pressure scale heights as the standard value. We assume that the initial metallicity of the star is $Z = 0.02$. We make use of the basic.net, coburn.net, and approx21.net nuclear networks in MESA. Radiative opacities are computed adopting tables from the OPAL project [Iglesias and Rogers (1996)[18]].

The effects of rotation on the equation for the transport of angular momentum have been accounted for according to the procedure described by the diffusion equation [Endal and Sofia (1978)[19]]. We take into account various instabilities induced by rotation that result in mixing: Eddington–Sweet circulation, dynamical and secular shear instability, and the Goldreich–Schubert–Fricke instability.

The variation of the chemical elements due to convection and rotation-induced mixing are also expressed as a diffusion equation. In this work, the thermohaline mixing effect is directly included in our models, so we consider its effect separately. Thermohaline mixing is treated to be a diffusion scheme (Wellstein *et al.*[20]). The corresponding diffusion coefficient is based on the works of Kippenhahn *et al.*,[21] Stern,[22] and Ulrich.[23]

An analytical prescription for the diffusion coefficient associated with internal gravity waves (IGWs) mixing was developed and implemented to interpret the Li and Be depletions in the Sun and other low-mass MS stars of different ages by Montalban and Schatzman.[24,25] To estimate the diffusivity from mixing by IGWs, we follow the approach of Montalban and Schatzman,[24,26] who found

$$D_{\rm M} = A^2 K^2 \frac{N}{2\pi}\left(\frac{\rho_0}{\rho}\right)^2\left(\frac{r_0}{r}\right)^{12} f^{-2} u_{\rm M}^5 \alpha_{\rm M}^{-1}, \tag{1}$$

where

$$f = \int_{r_0}^{r} K N^3 \left(\frac{r_0}{r^*}\right)^3 dr^*, \tag{2}$$

and quantities with subscripts of 0 are evaluated at the convective boundary. We assume the leading numerical constant $A^2 \sim 1$, which is the adjustable parameter and adopt a characteristic horizontal eddy scale $a_{\rm M} \sim 10^9$ cm. Other physical quantities have the same meaning as those found in literature.

The internal gravity wave mixing scenario in our study differs from Li *et al.*[11] Firstly, the diffusion coefficient given by Li *et al.*[11] is expressed as

$$D_{\rm M} = A\left[D_{\rm th} N \left(\frac{\rho_{\rm b}}{\rho}\right)\left(\frac{r_{\rm b}}{r}\right)^6\right]^2 V^{8n-3} l^{1-2n} f^{-2n}, \tag{3}$$

where $n = 2/3$. Secondly, we have employed internal gravity waves generated by convective turbulence inside stars during the first He flash. However, Li *et al.*[11] considered the action time of the mixing process induced by internal gravity waves under the frequency conditions $N^2 \gg \omega^2$. For stellar wind mass loss, we adopt Reimers[27] prescription (with $\eta_{\rm R} = 0.5$) from the ZAMS up to central helium exhaustion.

Results of Numerical Calculation. The initial mass of the system components was set from $1.3\,M_\odot$ to $1.7\,M_\odot$. The initial spin velocities are set to from 0 km/s to 150 km/s. The evolution is followed from the onset of central H burning to the core helium exhaustion.

Figure 1 shows evolutionary tracks for non-rotating and rotating models with different initial velocities and initial masses. The rotating models become less luminous and lower temperature at the onset of the evolution from zero age main sequence. This evolutionary feature can be attributed to the centrifugal force. The corresponding convective core can be significantly reduced due to a smaller core temperature. The centrifugal force counteracts part of gravity, reducing the core pressure and thus decreasing the central temperature. In rotating models, the turn-off is moved towards cooler temperatures while the luminosity is slightly enhanced. Rotation-induced mixing has also an important impact on the internal abundance profiles and it can enlarge the lifetime of main sequence with respect to those of non-rotating models. In fact, due to the positive slope of the hydrogen profile, mixing slightly feeds the core with fresh hydrogen fuel. The exhaustion of hydrogen in the central region is delayed and the time spent on main sequence increases. The luminosity of non-rotating stars is almost identical to the one of rotating ones after the main sequence [Fig. 1(b)]. The main reason is that the rotationally induced mixing can cause helium to diffuse from the core to the envelope and thus the opacity in the envelope can be reduced by the rotationally induced mixing.

Figure 2 shows that the profiles of the spin angular velocity at five different evolutionary stages for models with different initial rotational rates. We find that the profile of spin angular velocity approximately maintains a constant value during main sequence. The main reason is that we have adopted the Taylor–Spruit dynamo in our rotating models. Magnetic fields can enforce the solid body rotation in the star. It is very interesting that we compare the predicted rotational rates of the theoretical models with the observations of asteroseismology data at the RGB and HB stage. The data of asteroseismology indicates that the core of the red giants in these sample are rotating 5 to 10 times faster than their envelopes (Moyano *et al.*[28]). The theoretical results reveal that the rotational ratio of the core to the envelope is about 6.31 at the evolutionary point of red giant bump for the model with initial velocities $v_{\rm ini} = 100$ km/s. The core rotational rate of the bulk of RGB stars, which is in the range of $\Omega_{\rm c}/2\pi \sim 200$–1200 nHz (Gehan *et al.*[29]). The theoretical results show that the core rotation rate of the RGB is about 780 nHz at the red giant bump. The angular velocities of the helium core in horizontal branch stars are in order of 100 nHz. The theoretical results show that the core rotation rate of the horizontal branch is about 92 nHz for the model with the initial rotational rate $v_{\rm ini} = 100$ km/s. Our theoretical calculations are consistent with the astroseismology data.

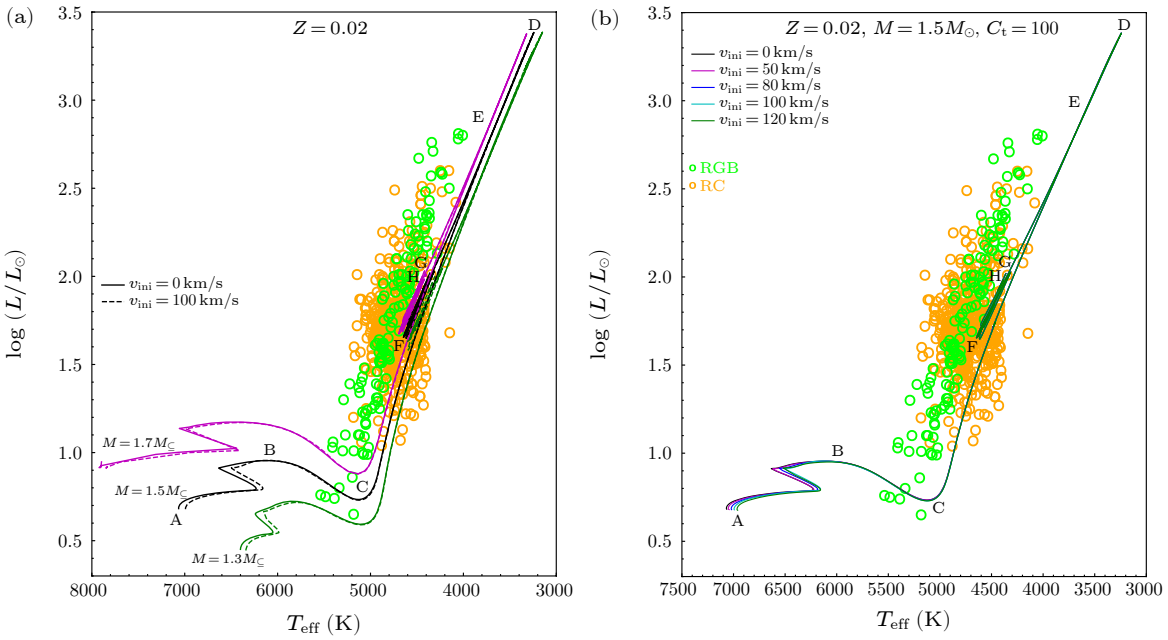

Fig. 1. Evolutionary tracks for non-rotating and rotating models with different initial stellar mass (a) the evolutionary tracks for with different initial velocities in the HR diagram (b). The observational data are from Bharat *et al.*,[30] Yan *et al.*,[5] and Buder *et al.*[31,32] Point A denotes zero age main sequence, point B represents the turn-off point of main sequence, point C is the stage of the first dredge-up, point D is the tip of red giant star. Points E, F, and G are the beginning, middle, and terminal of lithium enrichment. $C_{\rm t}$: thermohaline coefficient.

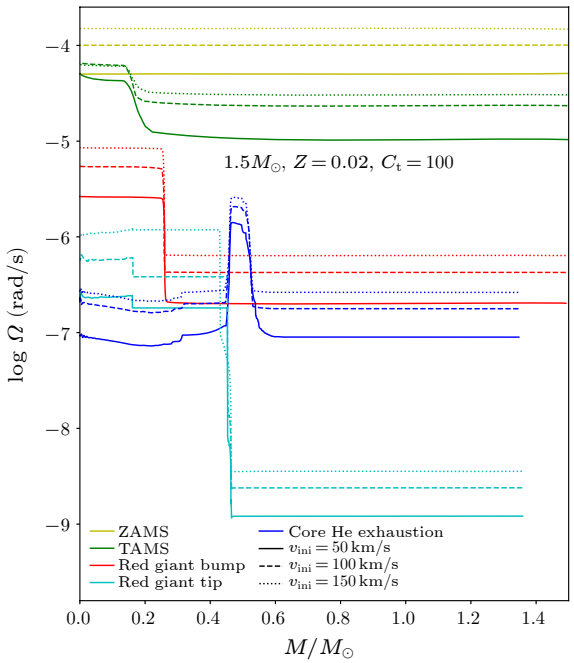

Fig. 2. Evolution of angular velocity profiles for the model 1.5 $M_\odot$ with different initial velocities. Each curve with different colors refers to a different epoch. The epoch has been indicated in the legend.

Figure 3 shows the evolution of stellar luminosity as a function of the surface lithium abundance A(Li). The lithium abundance A(Li) stays constant during the main sequence for the non-rotating model [see Fig. 3(a)]. After the non-rotating star 1.5 $M_\odot$ leaves the main sequence and crosses a region in the HR diagram known as the Hertzsprung gap (between end of core hydrogen burning and the base of the giant branch in Fig. 1), A(Li) starts to decrease from 3.4 to 0.8. This is because surface lithium is conveyed to the stellar interior due to the first dredge-up (hereafter, FDU). The first dredge-up is the first major mixing event in a lifetime of the star. The main reason is that the Li-depleted interior is diluted with the relatively rich exterior, decreasing its abundance in the non-rotating star. The surface abundance changes expected due to the FDU are increases in the abundances of ^{3}He, ^{4}He, ^{13}C, and ^{14}N, and decreases (due to dilution) in the abundances of ^{1}H, ^{12}C, ^{7}Li, ^{7}Be, and ^{16}O. Surface ^{3}He and ^{7}Li are anticorrelated because the pp-Ⅱ branches fuse ^{3}He with pre-existing ^{4}He to form ^{7}Be. The lithium can be produced via the nuclear reaction $^7\mathrm{Be}+e^- \rightarrow {}^7\mathrm{Li}+\nu_{\rm e}+\gamma$.

First dredge-up leaves behind an abundance discontinuity that becomes very important for subsequent evolution. This discontinuity is believed to inhibit any extra mixing between the hydrogen shell and envelope. The hydrogen shell will move out (in mass) until it eventually reaches the hydrogen discontinuity left behind by the FDU. The amount of available fuel and the opacity of the hydrogen shell increases and the rate of hydrogen burning drops, which causes a drop in luminosity but a rise in effective temperature. This is the main reason for the formation of the red giant star bump.

In the rotating models, the abundance gradients are smoothed out compared to the non-rotating star. ^{3}He, ^{13}C, and ^{14}N diffuse outwards, while ^{12}C and ^{18}O diffuse inwards during main sequence. Rapid rotation can cause these chemical elements to change significantly (see Figs. 3 and 4). Compared to the non-rotational model, surface lithium depletion starts earlier (i.e., at a higher effective temperature) [see Fig. 3(a)]. In rotating stars, however,

rotationally induced mixing causes a downward transport of lithium during the main sequence. The element lithium is transported into layers where the temperature is sufficiently high to destroy it. This leads to a depletion of lithium by the rotationally induced mixing during main sequence. The faster the rotational mixing in the envelope, the stronger the depletion because of a faster meridional circulation [see Fig. 3(a)]. The main reason is that the diffusion coefficient (and efficiency) due to meridional (Eddington–Sweet) circulation that characterizes this mixing increases with the rotational rate. Meridional circulations which are a consequence of the baroclinic instability are only associated with the square of angular velocity.

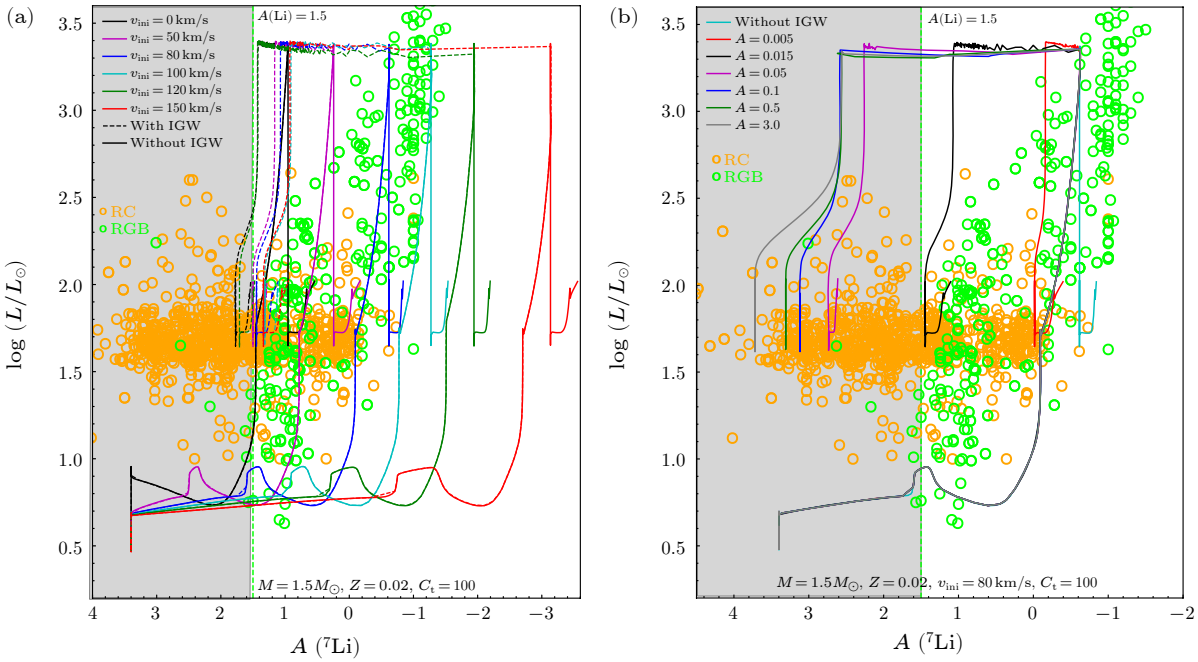

Fig. 3. Stellar luminosity as a function of lithium abundance in stars for different models: (a) for the models with different initial rotational velocities, (b) for the models with different parameter A. The yellow circles are red clump stars and the green ones are red giant stars. They are screened by Bharat *et al.*[30]

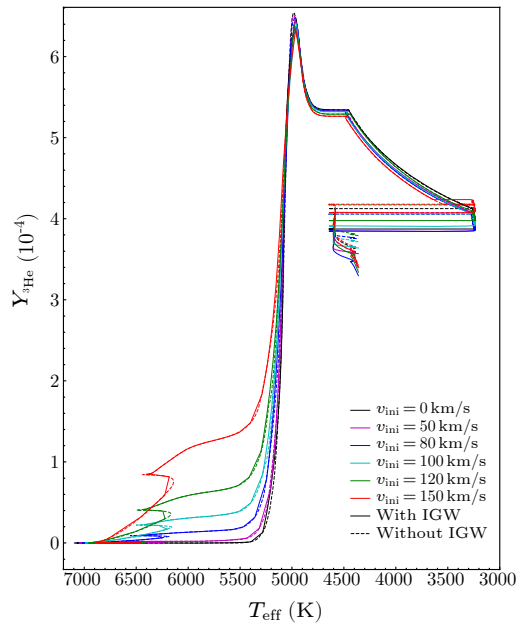

Fig. 4. Surface abundance of ^{3}He as a function of the effective temperature for the models with different initial velocities.

Low-mass red-giant-branch (RGB) stars show evidence of extra-mixing operating in their radiative zones between the hydrogen-burning shell and convective envelope that starts above the so-called red giant bump. When the thermohaline mixing sets in at the bump of red giant stars, it transfers ^{3}He from the convective envelope down to the hydrogen-burning shell. This leads to a rapid decrease of the surface abundance of ^{3}He as can be seen in Fig. 4. Therefore, the thermohaline mixing enormously reduces the ^{3}He and ^{7}Li abundances, which may affect the ^{7}Li production after the RGB tip.

We find from Fig. 4(a) that without the IGW induced mixing, the non-rotating star has no lithium enrichment after central helium ignition. The enrichment of Li mainly occurs from the RGB tip under the action of IGW induced mixing [see Fig. 3(a)]. The abundance of lithium-rich red clump stars depends on three important physical factors: the lithium abundance at the tip of red giant stars, the diffusion coefficient produced by the helium flash induced IGW mixing, and the duration of the lithium enhancement. The rotational and the thermohaline mixing tend to reduce the lithium ^{7}Li and ^{3}He abundances at the tip of red giant stars. Therefore, both of them are not beneficial to enhance the lithium abundance from the tip of red giant star [see Fig. 3(a)]. However, the enrichment amplitude of lithium abundance in faster rotating stars is greater than that of slower rotating or non-rotating stars. For example, surface lithium abundance increases about $\Delta A = 0.694$

for the non-rotating $1.5\,M_\odot$, whereas it goes up about $\Delta A = 2.89$ for the rotating star with $v_{\rm ini} = 100\,{\rm km/s}$. The main reason is that rapid rotation greatly increases the enrichment time or the lifetime during the core helium burning. For example, the duration of lithium enrichment is 0.221 Myr for the non-rotating star while it is 0.242 Myr for the rotating star with $v_{\rm ini} = 100\,{\rm km/s}$. The main reason is that rotationally induced mixing can enlarge the helium core mass. The helium core mass is $0.463\,M_\odot$ for the non-rotating stars whereas it is $0.465\,M_\odot$ for the rotating star with $v_{\rm ini} = 100\,{\rm km/s}$. It is well known that the efficiency of diffusion process depends heavily on the diffusion coefficient. The greater the diffusion coefficient, the higher the diffusion efficiency. Diffusion coefficient depends on the adjustable parameter A for the IGW in Eq. (1). When the parameter A in the diffusion coefficient of the IGW induced mixing can reach 0.015, it governs the thermohaline mixing and other rotationally induced instabilities, and can be responsible for the mixing of the chemical elements. When the parameter A can reach as large as 0.1, the increase of Lithium abundance will attain about 3.0 dex. An increase in the diffusion coefficient could lead to more Li enrichment. We have calculated it for the case of $A = 3$. The lithium abundance $A_{\rm Li}$ can approximately reach the value of 3.72 dex. Therefore, our models can explain the super lithium-rich red clump stars with $A({\rm Li}) > 3.3$ if the diffusion coefficient is larger than 10^{12} (i.e., $A > 0.5$).

Denissenkov and Weiss[33] investigated the effect of rotation-induced mixing (i.e., rotation-driven meridional circulation and turbulent diffusion) on the surface lithium abundance using the diffusion coefficients $D_{\rm mix}$. They also found that the corresponding diffusion coefficient of $D_{\rm mix}$ (10^8 to $10^{10}\,{\rm cm^2{\cdot}s^{-1}}$) were too low to lead to lithium enrichment and invoked the engulfing of a planet in order to trigger the transport process. The diffusion coefficient for IGW mixing driven by the IGW was expected to increase with the luminosity as $D_{\rm IGW} \approx f(L)K$, where $f(L) \propto L^{4/3}$. One can obtain the estimate of $D_{\rm IGW}(L_{\rm tip}) \sim 2.4 \times 10^{11}\,{\rm cm^2/s}$ at the RGB tip because the corresponding luminosity is $\log(L/L_\odot) = 3.4$. We have obtained the theoretical value of $D_{\rm IGW}(L_{\rm tip}) \sim 2.55 \times 10^{11}\,{\rm cm^2/s}$ in this study. Therefore, their results are consistent with ours.

The main conclusion are as follows: (1) The flash induced IGW mixing is mainly triggered by turbulent convective motions. The larger luminosity produced by the helium flash can provide a larger diffusion coefficient, which can explain the super lithium-rich red clump stars. For red clump stars, the flash induced IGW mixing can reproduce the observed data very well. (2) Thermohaline mixing is confirmed to be the primary physical process governing the surface abundances of ^{3}He and ^{7}Li for stars more evolved than the RGB bump. Thermohaline mixing in low-mass giants is capable of reducing large quantities of ^{3}He and ^{7}Li. Therefore, it does not favor the surface enrichment of ^{7}Li. (3) Rotation may play a role in setting the surface ^{7}Li abundance on the MS and RGB. Rapid rotation tends to reduce the lithium enrichment on the red giant branch. However, it can also increase the efficiency of the flash induced IGW mixing because rotational mixing can increase the duration of the flash induced IGW mixing.

Acknowledgments. This work was supported by the National Natural Science Foundation of China (Grant Nos. 11863003 and 12173010), and the Science and Technology Plan Projects of Guizhou Province (Grant No. [2018]5781).

References

[1] Li Z, Song H F, and Peng W G 2018 *Chin. Phys. Lett.* **35** 079701
[2] Zhang J, Ma R Y, Li H J, Zhang B *et al.* 2017 *Chin. Phys. Lett.* **34** 049701
[3] Pols O R, Schröder K P, Hurley J R, Tout C A, and Eggleton P P 1998 *Mon. Not. R. Astron. Soc.* **298** 525
[4] Yan H L and Shi J R 2022 *Chin. Astron. Astrophys.* **46** 1
[5] Yan H L, Shi J R, Zhou Y T *et al.* 2018 *Nat. Astron.* **2** 790
[6] Martell S L, Simpson J D, Balasubramaniam A G *et al.* 2021 *Mon. Not. R. Astron. Soc.* **505** 5340
[7] Yan H L, Zhou Y T, Zhang X F *et al.* 2021 *Nat. Astron.* **5** 86
[8] Aguilera-Gómez C, Chanamé J, Pinsonneault M H, and Carlberg J K 2016 *Astrophys. J.* **829** 127
[9] Ashwell J F, Jeffries R D, Smalley B *et al.* 2005 *Mon. Not. R. Astron. Soc.* **363** L81
[10] Charbonnel C and Balachandran S C 2000 *Astron. Astrophys.* **359** 563
[11] Li X F, Shi J R, Li Y, Yan H L, and Zhang J H 2023 *Astrophys. J.* **943** 115
[12] Paxton B, Bildsten L, Dotter A, Herwig F, Lesaffre P, and Timmes F 2011 *Astrophys. J. Suppl.* **192** 3
[13] Paxton B, Cantiello M, Arras P *et al.* 2013 *Astrophys. J. Suppl.* **208** 4
[14] Paxton B, Marchant P, Schwab J *et al.* 2015 *Astrophys. J. Suppl.* **220** 15
[15] Paxton B, Schwab J, Bauer E B *et al.* 2018 *Astrophys. J. Suppl.* **234** 34
[16] Böhm-Vitense E *et al.* 1958 *Z. Astrophys.* **46** 108
[17] Cox and Giuli 1968 *Principles of Stellar Structure* (New York: Gordon and Breach)
[18] Iglesias C A and Rogers F J 1996 *Astrophys. J.* **464** 943
[19] Endal A S and Sofia S 1978 *Astrophys. J.* **220** 279
[20] Wellstein S, Langer N, and Braun H 2001 *Astron. Astrophys.* **369** 939
[21] Kippenhahn R, Ruschenplatt G, and Thomas H C 1980 *Astron. Astrophys.* **91** 175
[22] Stern M E 1960 *Tellus A* **12** 172
[23] Ulrich R K 1972 *Astrophys. J.* **172** 165
[24] Montalban J 1994 *Astron. Astrophys.* **281** 421
[25] Montalban J and Schatzman E 2000 *Astron. Astrophys.* **354** 943
[26] Montalban J and Schatzman E 1996 *Astron. Astrophys.* **305** 513
[27] Reimers D 1975 *Memoires of the Societe Royale des Sciences de Liege* **8** 369
[28] Moyano F D, Eggenberger P, Mosser B, and Spada F 2023 *Astron. Astrophys.* **673** A110
[29] Gehan C, Mosser B, Michel E *et al.* 2018 *Astron. Astrophys.* **616** A24
[30] Kumar Y B, Reddy B E, Campbell S W, Maben S, Zhao G, and Ting Y S 2020 *Nat. Astron.* **4** 1059
[31] Buder S *et al.* 2018 *Mon. Not. R. Astron. Soc.* **478** 4513
[32] Buder S, Sharma S, Kos J *et al.* 2021 *Mon. Not. R. Astron. Soc.* **506** 150
[33] Denissenkov P A and Weiss A 2000 *Astron. Astrophys.* **358** L49